


RESEARCH

Open Access



# Enhancing indoor air quality and thermal comfort in indoor swimming pool facilities: investigating the impact of ventilation system configurations

Ahmed M. Hanafi<sup>1\*</sup> , Mohamed A. Ibrahim<sup>1</sup>, Taher M. Abou-deif<sup>2</sup> and Samy M. Morcos<sup>2</sup>

\*Correspondence:  
ahmedhanafi.eng@o6u.edu.eg

<sup>1</sup> Department of Mechatronics Engineering, Faculty of Engineering, October 6 University, Giza, 6Th of October City, Egypt

<sup>2</sup> Department of Mechanical Power Engineering, Faculty of Engineering, Cairo University, Giza, Egypt

## Abstract

This study focuses on enhancing indoor air quality and thermal comfort in indoor swimming pool facilities through the investigation of ventilation system configurations. Creating a comfortable and healthy environment in these facilities is crucial for the well-being of occupants and overall operational efficiency. The performance of the ventilation system significantly influences user comfort, energy consumption, and air quality. This research aims to analyze the impact of different ventilation system configurations on indoor air quality and thermal comfort parameters using computational fluid dynamics (CFD) simulations.

To achieve the research objectives, CFD simulations were conducted using ANSYS Fluent<sup>®</sup>, a widely used commercial CFD package. The simulations involved solving the governing equations for continuity, momentum, energy, and species transport, along with employing the k-epsilon turbulence closure model. A high-resolution mesh with over 5.6 million elements accurately captured the flow regimes and related phenomena.

The study investigated various aspects of ventilation system configurations, including the placement and design of inlets and outlets, airflow rates, and distribution patterns. Evaluations were made based on key performance indicators such as indoor air quality parameters, thermal comfort indices, and energy efficiency metrics. Comparisons were made between different configurations to identify the most effective strategies for enhancing indoor air quality and thermal comfort.

The findings of the study demonstrate the importance of ventilation system design in achieving optimal indoor air quality and thermal comfort in indoor swimming pool facilities. The results indicate that specific configuration choices, such as the use of circular inlets in the ceiling for improved spectator comfort and rectangular inlets in the side walls for better performance in the swimming pool area, can significantly impact thermal conditions and air distribution. Additionally, the study emphasizes the need for appropriate inlet grille height to ensure adequate air mixing and thermal comfort.

The outcomes of this research provide valuable insights for architects, engineers, and facility managers involved in the design, construction, and operation of indoor swimming pool facilities. By understanding the impact of different ventilation system configurations, stakeholders can make informed decisions to optimize indoor air quality, thermal comfort, and energy efficiency. Ultimately, this research contributes to the development of sustainable and comfortable indoor swimming pool environments that cater to the needs of occupants and enhance their overall experience.

**Keywords:** CFD simulation, Air conditioning, Spectator comfort, Flow regimes, Passive building design, Olympic sports, Swimming pool, Water evaporation rate

## Introduction

In sports pools, the swimming area is not the only major component; grandstands and spectator seating also occupy a significant portion. To ensure the comfort of the spectators, efficient and reliable air conditioning is necessary, in addition to maintaining a comfortable environment around the swimming pool. Dehumidification of the moist air is essential to achieve this goal.

The high-water evaporation rate necessitates the 24-h operation of the air conditioning system, regardless of the pool hall's intensity of use. An intelligently designed and controlled system is ideal for regulating the air conditioning system. The complexity of indoor swimming pool air conditioning systems requires appropriate sizing to ensure a consistently good climate. The efficiency of fan motors used is critical, especially for larger volumes.

Sports pools are typically operated by local authorities or the state, making operating costs a significant consideration. The modernization of outdated air-conditioning technology can significantly reduce operating costs. Buildings designed and constructed by passive building criteria can achieve energy savings of over 50% compared to standard designs. When planning a sports swimming pool, future demands must be considered during the planning phase.

Indoor air quality (IAQ) and thermal comfort are important elements in occupant well-being and productivity in indoor spaces. Various methods have been developed to handle these issues extensively, ranging from complex Computational Fluid Dynamics (CFD) simulations to simpler yet effective ways that give vital insights into IAQ and thermal comfort factors.

While CFD is well-known for its ability to capture complicated flow patterns and spatial changes inside interior environments, it necessitates a large amount of processing power and specialized knowledge. However, there are various simpler ways, each with distinct benefits in assessing IAQ and thermal comfort:

Multizone models split a building into interconnected zones that interact with one another. These models give a more manageable way to evaluate IAQ and thermal comfort by reducing the intricacies of airflow and temperature distribution. While they may not catch fine details, they do provide practical knowledge of the broader situation.

Multizone air parameter models offer both advantages and problems. Their high calculation speed is one benefit, making them excellent for creating airflow and energy performance models [1]. However, the assumption of well-mixed air in a zone might restrict the accuracy of multizone models. This constraint can be solved by employing

Computational Fluid Dynamics (CFD) models, which are better suited to areas where the well-mixed assumption does not apply [2]. Another problem is that the outputs of multizone models may differ from the observed behaviour of a real-world building owing to input mistakes or uncertainties. Calibration of the models based on measurements in the actual building is required to overcome this. Overall, multizone models provide high calculation speed and are suitable for a wide range of applications, although their accuracy may be limited in some cases.

Empirical models use historical data and observations from the actual world to determine correlations between important factors and comfort feelings. These models are especially useful for short assessments and can give vital information about possible comfort concerns.

There are various advantages and downsides to using empirical models of air characteristics. One advantage is that they may use real-world air quality data to give a data-driven method to estimating pollutant concentrations. These models may also be used in conjunction with monitoring to develop acceptable air quality plans and evaluate emission reduction strategies [3]. Furthermore, the incorporation of microscale factors into empirical models has shown promise in terms of boosting prediction accuracy and performance. Empirical models, on the other hand, may obscure the physical rules that regulate the behaviors and interactions of contaminants, limiting our comprehension of the underlying mechanisms.

Furthermore, extensively parameterized empirical models may be unstable, especially when anticipating very nonlinear reactions [4]. Despite these limitations, empirical models can increase air quality management efficiency and give the geographical distribution of pollutant concentrations.

Direct monitoring of IAQ parameters via sensors gives real-time data on contaminants, humidity, and temperature. While not as complete as CFD models, this approach provides instant feedback on interior environmental conditions and is useful in detecting abrupt changes that may impair occupant comfort and well-being.

Monitoring indoor air quality and air parameters has various advantages. It aids in the reduction of health hazards associated with poor air quality. It enables better ventilation in enclosed places, which can considerably lower infection risk, as shown during the COVID epidemic [5]. Indoor air quality monitoring is especially critical for vulnerable groups like the elderly, children, and individuals with respiratory allergies. It is capable of measuring a wide range of air contaminants and chemicals, giving significant data for analysis and processing. Furthermore, indoor air quality monitoring systems may be configured to offer real-time data, warnings for exceeding thresholds, and internet access for analysis [6]. However, there are some drawbacks to consider. Traditional air-quality monitoring devices can be costly, inflexible, and provide only limited access to sensed data. Existing market equipment may only test a limited number of indoor air quality indicators and need costly consumables and annual maintenance services. Furthermore, systematic methods for these systems, as well as sophisticated air-quality monitoring devices capable of sensing pollutant concentrations in the air, are required. In conclusion, indoor air quality monitoring has several benefits in terms of health, enhanced ventilation, and data analysis. However, there are costs, restricted data availability, and the necessity for methodical standards and smart monitoring systems.

By including these simplified approaches into the study's framework, the relevance of practicality and accessibility in analysing IAQ and thermal comfort is acknowledged. These methods not only give basic insights, but also act as helpful tools for highlighting areas of concern that may deserve further examination using sophisticated techniques like CFD simulations.

### Previous research

Foncubierta Blázquez et al. [7] investigate the use of Computational Fluid Dynamics (CFD) techniques for modeling the evaporation rate of indoor swimming pools. To improve the precision of the numerical simulation, the study proposes an experimental adjustment of the turbulent Schmidt number ( $Sc_t$ ). The methodology describes the refined approach and modifies  $Sc_t$  based on wind tunnel experiment data. The results' accuracy is validated by comparing them to experimental data from previous studies. The study's findings suggest that when using CFD techniques to model the evaporation rate of indoor swimming pools, using a constant  $Sc_t$  value of 0.2 yields the most precise results.

Hanafi et al. [8] investigate the impact of air curtain flows on heat and mass transfer within an indoor swimming pool facility. Using the k-epsilon model, computational fluid dynamics (CFD) simulations are used to solve the governing equations for energy, species transport, and turbulence closure. The geometry of a semi-Olympic pool at Bishop's University in Sherbrooke, Quebec, Canada, with dimensions of 34.5 m × 25 m × 8 m and a coarsely trapezoidal shape, is modeled using SpaceClaim 3D software. The study also investigates the effect of the number and location of ventilation and air conditioning supply systems. The simulation results have been validated against OpenFOAM software and show good agreement. This study sheds light on the effects of air curtain flows on indoor pool environments, providing useful guidance for the design and operation of air conditioning systems in swimming pools.

Gabriel and Jessica [9] used computational fluid dynamics (CFD) simulations to evaluate ventilation efficiency in an indoor swimming pool. The study found that alternative air distribution concepts could improve ventilation efficiency and indoor air quality. The results of the presented CFD simulations indicate that the ventilation efficiency in the examined swimming pool could be improved with alternative air distribution concepts identified to provide better ventilation efficiency. A simple improvement could be to change the swirl diffusers from horizontally discharging to vertically discharging.

Ciuman and Lipska [10] examined the relevance of ventilation systems in indoor swimming pools and their influence on the building's correct functioning, user comfort, operational expenses, and safety. The article seeks to empirically identify the physical phenomena happening in a real indoor swimming pool and assess if the numerical model of the facility, produced with the use of Ansys CFX 14.5 software, accurately mapped these phenomena and how it should be improved in this sector. The study also examines the difficulty in determining the most accurate method for estimating moisture emission from the surface of the water in an indoor swimming pool. The numerical model was enhanced with the use of the authors' own approach of calculating moisture emission from the surface of the water. The revised numerical model was able to

simulate the actual circumstances in the indoor swimming pool with excellent concordance of the experimental and projected values.

Piotr et.al. [11] introduced a new method for assessing thermal comfort in indoor spaces using CFD numerical prediction. It determines the percentage of occupied zone cross-section area where thermal comfort criteria are satisfied. The method uses criteria like Lancaster-Castens-Ruge’s sultriness curve, PMV, PPD, DR, and ADPI to evaluate thermal comfort. The results show that the proposed method is effective in determining the percentage of satisfied criteria and can help design ventilation or air-conditioning systems. Additionally, it identifies areas for improvement.

Blázquez et al. [12] proposed a novel method for approximating water evaporation rates in indoor swimming pools. Three experiments were conducted on scaled models using test chambers, with the final experiment being performed in an actual swimming pool. The average relative error concerning experimental data was 8.9%.

The thermodynamic properties of each component and the mass diffusivity of water vapor in air are depended on temperature and pressure as follows [13, 14]:

$$D_{AB} \propto \left( \frac{T^{2.072}}{P} \right) \tag{1}$$

$$D_{H_2O-Air} = 1.87 \times 10^{-10} \left( \frac{T^{2.072}}{P} \right) m^2/s, 280K < T < 450K \tag{2}$$

Furthermore, for the evaluation of saturation vapor pressure ( $P_{v,s}$ ) as a function of temperature the following expression has been used [15]:

$$P_{v,s} = 10^5 \exp \left[ 65.832 - 8.2 \ln(T_s) + 5.717 \times 10^{-3} - \frac{7235.46}{T_s} \right] \tag{3}$$

Particularly, for stationary conditions it can be expressed as follows:

$$\dot{m}_e(t) = \left( \int_{A_{out}} \rho Y \vec{v} \cdot \hat{n} dA \right) - \left( \int_{A_{in}} \rho Y \vec{v} \cdot \hat{n} dA \right) \tag{4}$$

where:

$\rho$  is the density of humid air ( $kg/m^3$ ),  $Y$  is the water vapor mass fraction (kg of water vapor/kg of humid air),  $v$  is the fluid velocity,  $\hat{n}$  is the unit normal vector to the inlet ( $A_{in}$ ) and outlet ( $A_{out}$ ) surfaces of the control volume.

In mixed convection settings, where the numerical/experimental ratio is 1.010.010, the relative errors of the water evaporation rate with respect to experimental values are reduced, according to the study’s findings. Conditions, where forced convection predominates, are characterized by the largest error dispersion.

M. M. Shah [16]: studied the approaches for an estimate of the evaporation rate of water vapor from water surfaces. The study presented and discussed the correlations between enclosing crowded and uncrowded water pools Including approaches offered for both types.

- Unoccupied swimming pool

- Use a larger mass flow rate between Equations 5 and 6

$$E_0 = C \rho_w (\rho_r - \rho_w)^{\frac{1}{3}} (W_w - W_r) \quad (5)$$

$$E_0 = b(p_w - p_r) \quad (6)$$

- Occupied swimming pool

$$\frac{E_{occ}}{E_0} = 1.9 - 21(\rho_r - \rho_w) + 5.3N^* \quad (7)$$

Where :

$E_o$  = rate of evaporation from an occupied swimming pool,  $\frac{\text{kg}}{\text{m}^2 \cdot \text{h}}$   
 $E_{occ}$  = rate of evaporation from an occupied swimming pool  $\frac{\text{kg}}{\text{m}^2 \cdot \text{h}}$   
 $p$  = partial pressure of water vapor in the air, Pa  
 $W$  = specific humidity of the air, kg of  $\frac{\text{moisture}}{\text{kg}}$  of air  
 $\rho$  = density of air, the mass of dry air per unit volume of moist air,  $\frac{\text{kg}}{\text{m}^3}$   
 $r$  = at room temperature and humidity  
 $w$  = saturated at water surface temperature  
 $N$  = the number of occupants per unit pool area  
 $C = 35$   
 $b = 0.00005$

Mohamed Abo Elazm et al. [17] investigated the influence of air velocity and evaporation rate on the indoor air quality of an enclosed swimming pool hall, specifically the San-Stefano Grand Plaza swimming pool in Alexandria, Egypt. The study analyzed the effects of altering the supply air velocity and temperature on the rate of evaporation using computational fluid dynamics (CFD) modelling.

The results of the study indicated that the smaller temperature difference between the air and water contributed to an increase in the rate of evaporation from the surface of the swimming pool. In addition, the simulation findings revealed that the supply air velocity and temperature had a substantial impact on the evaporation rate, and that improving these parameters could improve the indoor air quality of enclosed swimming pools.

In addition, increased air velocity led to a decrease in relative humidity and temperature, which could improve the internal air quality of enclosed swimming pools. The findings of this study provide important insights into the elements that influence the interior air quality of swimming pool halls and can inform the creation of methods to optimize the air quality in these environments.

### Presented study

A. Limane et al. [18]: simulated the 3D airflow with mass and heat transport in a complex indoor swimming pool using the OpenFOAM software. Comparing the airflow properties revealed excellent concordance. Two simulations were conducted with summer and winter as their respective boundary conditions. Their study revealed a

negligible effect on the inner situation exhibited by a greater temperature differential in winter. In addition, the impact of swimmers on the atmosphere was assessed and determined to be of enormous significance.

The study demonstrated that the OpenFOAM algorithm can replicate this 3D model airstream with mass and heat transport. Consequently, CFD modeling investigations of environments in large volumes with HVAC can be conducted cheaply. The numerical results obtained by modifying RANS turbulence models are acceptable. However, the model k- $\epsilon$  Launder & Sharma yields the most acceptable results. This innovative approach reframed the evaporation rate as pertaining to a thin layer of air immediately above the pool's water surface. Within this conceptual framework, the relative humidity was established at 100% RH, and the temperature mirrored that of the water pool. Notably, this characterization of the evaporation rate disregarded the consideration of mass flow rate, emphasizing a focused analysis of air–water interactions in the evaporation process. This novel definition showcases the study's commitment to discerning the fundamental mechanisms governing indoor air quality and thermal dynamics, even in the absence of certain intricate parameters.

### Swimming pool description

This research focuses on a semi-Olympic pool at Bishop's University in Sherbrooke (Quebec, Canada). Considered is a big enclosure with complex geometry, roughly trapezoidal in shape and measuring (34.5 m, 25 m, 8 m) in size. As illustrated in Fig. 1, the enclosure comprises of the water basin area and the spectator stands, which are partially isolated from one another. Actual geometry. It has two partially subterranean exterior walls on the north and west sides, as well as two interior walls on the east and south sides.

The HVAC (heating, ventilation, and air conditioning) system is solely responsible for maintaining the pool's air temperature. Due to the numerous inlets and outputs of the ventilation system, the flow field within the pool is complex. As shown in Fig. 2, the water basin area is covered by a false ceiling comprised of six horizontal parts at varying heights (a). On its sloped parts, there are three rows of air inlets, with each row containing six air inlets (1.05 m  $\times$  0.19 m) that introduce air at a 30° angle from the horizontal plane. The air exits (1.20 m  $\times$  0.60 m) are located on the opposite (north) side of the three rows of air inlets at the top of a single horizontal segment. The spectator stands are covered by a long fake ceiling and have six air inlets (measuring 0.3 m  $\times$  0.3 m) that admit air at a 30° angle from the horizontal plane on three sides.

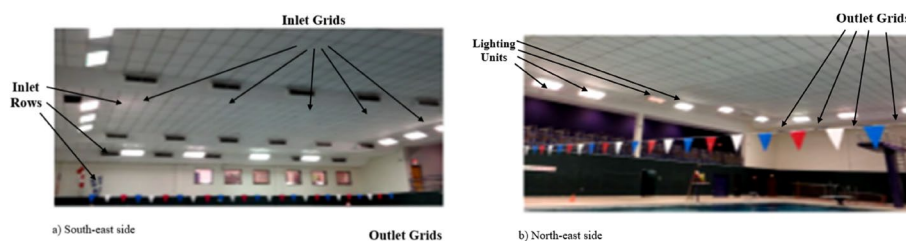


**Fig. 1** The real geometry of the swimming pool [19]



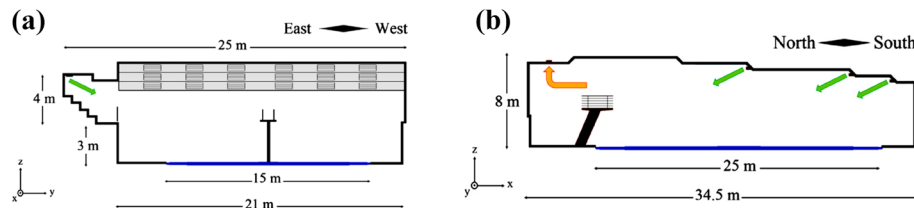


**Fig. 2** Pool dimensions and ventilation inlets/outlets: **a** Cross-section displaying spectator stands **b** False ceiling longitudinal section [18]

**Methods**

Computational fluid dynamics (CFD) is a highly effective tool for analyzing fluid dynamics. This computer-based simulation technique provides an approximate solution to the equations governing fluid motion in two or three dimensions. The technique involves dividing the region of flow into a large number of smaller domains, known as mesh or grid cells. CFD can handle complex geometries and time-dependent flows with ease. The resulting solution consists of values of flow parameters such as velocity or gas concentration, calculated at each of the grid cells, which provides a comprehensive and time-dependent picture of the fluid flow. CFD is a computer-based tool for simulating the behavior of a system involving fluid flow, heat transfer, and other related physical processes. It works by solving the equations for the conservation of mass, momentum, turbulence, and energy at every cell over a region of interest with prescribed (known) conditions on the boundary of the region. Commonly known as the Navier-Stokes equation, these equations are highly non-linear partial differential equations that describe the fundamental behavior of the fluid. Because these equations cannot solve in a closed form, this CFD software employs what are known as "differencing" techniques to derive approximate solutions to the equations throughout the geometry modeled. CFD makes use of computer simulation to obtain an approximate solution of the governing equations of fluid flow.

Numerical methods were employed to model airflow characteristics in the swimming pool hall CFD simulation. These complex computer programmes use the basic equations of mass, momentum, and energy conservation, given below in Cartesian coordinates for familiarisation [20, 21].

- Continuity equation with three-dimensional

$$\frac{\partial \rho}{\partial t} + \frac{\partial(\rho u)}{\partial x} + \frac{\partial(\rho v)}{\partial y} + \frac{\partial(\rho w)}{\partial z} = 0 \tag{8}$$

- Three momentum equations in Cartesian x, y, and z coordinates

$$\rho \frac{Du}{Dt} = \rho g_x - \frac{\partial P}{\partial x} + \frac{\partial \tau_{xx}}{\partial x} + \frac{\partial \tau_{yx}}{\partial y} + \frac{\partial \tau_{zx}}{\partial z} \tag{9}$$

$$\rho \frac{Dv}{Dt} = \rho g_y - \frac{\partial P}{\partial y} + \frac{\partial \tau_{xy}}{\partial x} + \frac{\partial \tau_{yy}}{\partial y} + \frac{\partial \tau_{zy}}{\partial z} \tag{10}$$



$$\rho \frac{Dw}{Dt} = \rho g_z - \frac{\partial P}{\partial z} + \frac{\partial \tau_{xz}}{\partial x} + \frac{\partial \tau_{yz}}{\partial y} + \frac{\partial \tau_{zz}}{\partial z} \quad (11)$$

• Energy equation

$$\rho \frac{\partial h}{\partial t} + \rho u \frac{\partial h}{\partial x} + \rho v \frac{\partial h}{\partial y} + \rho w \frac{\partial h}{\partial z} = \frac{\partial}{\partial x} \left[ k \frac{\partial T}{\partial x} \right] + \frac{\partial}{\partial y} \left[ k \frac{\partial T}{\partial y} \right] + \frac{\partial}{\partial z} \left[ k \frac{\partial T}{\partial z} \right] + \varnothing \quad (12)$$

Where :

$k$  = Thermal conductivity coefficient,  $W/m^{\circ}C$

$h$  = Enthalpy,  $kJ/kg$

$\rho$  = Density,  $kg/m^3$

$p$  = Pressure,  $Pa$

$t$  = Time,  $s$

$T$  = Drybulb Temperature of gas mixture,  $K$

$g$  = Gravitational acceleration,  $m/s^2$

$x, y, z$  = Cardinal coordinate components

$u$  = Instantaneous velocity component in  $x$  direction,  $m/s$

$v$  = Instantaneous velocity component in  $y$  direction,  $m/s$

$w$  = Instantaneous velocity component in  $z$  direction,  $m/s$

$\tau_{ij}$  = Subgrid – scale stress

### Numerical validation

This study aims to validate the results of ANSYS Fluent with previous experimental and numerical work of A. Limane et al. [18]. The work of A. Limane et al. used to validate the numerical results with the experimental results by simulations of the 3D airflow using OpenFOAM software. The Present comparisons between the numerical results using ANSYS Fluent Software to those previously published experimental and numerical results obtained by different researchers in the field using OpenFOAM software.

### Boundary conditions

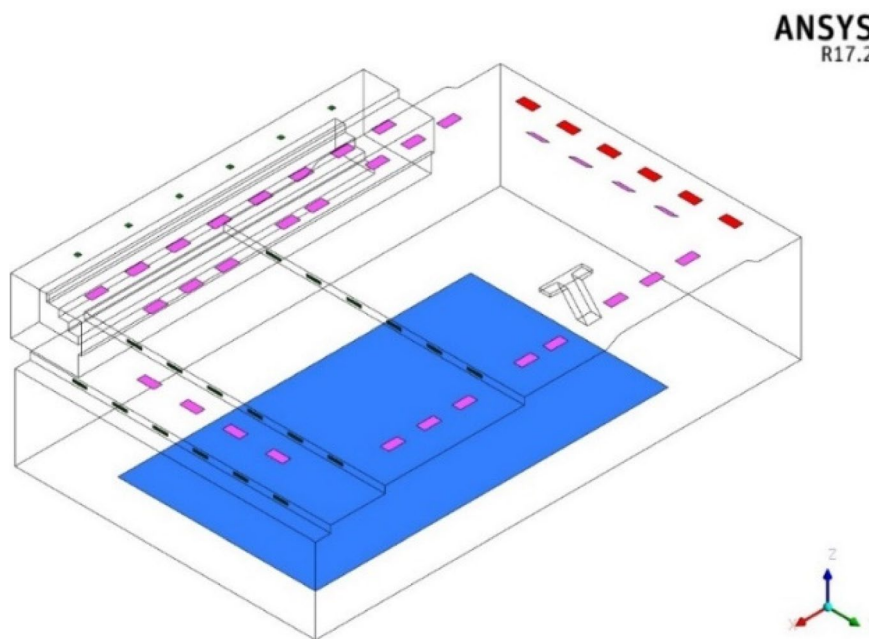
Figure 3, an isometric view of the swimming pool hall, provides a visual representation of the original configuration of the swimming pool hall.

### Grid independency check

Several runs of the initial CFD model were performed on various mesh sizes, and their results were compared to analyses of the solution's grid independence [22]. The grid independency check was accomplished through comparisons of the same configuration for different grid sizes of 3.5, 5.6, 6.9, and 10 million. The comparison is conducted using a line plot, as illustrated in Fig. 4.

### Mesh quality

The quality of the mesh used for computational fluid dynamics (CFD) simulations was carefully considered. ANSYS Fluent 17.2 provides recommendations regarding mesh quality, advising against low orthogonal quality or high skewness values [23]. Table 1




■ Swimming pool ■ Inlet grille ■ Outlet grille ■ Lighting unit  
**Fig. 3** Isometric view of the swimming pool hall

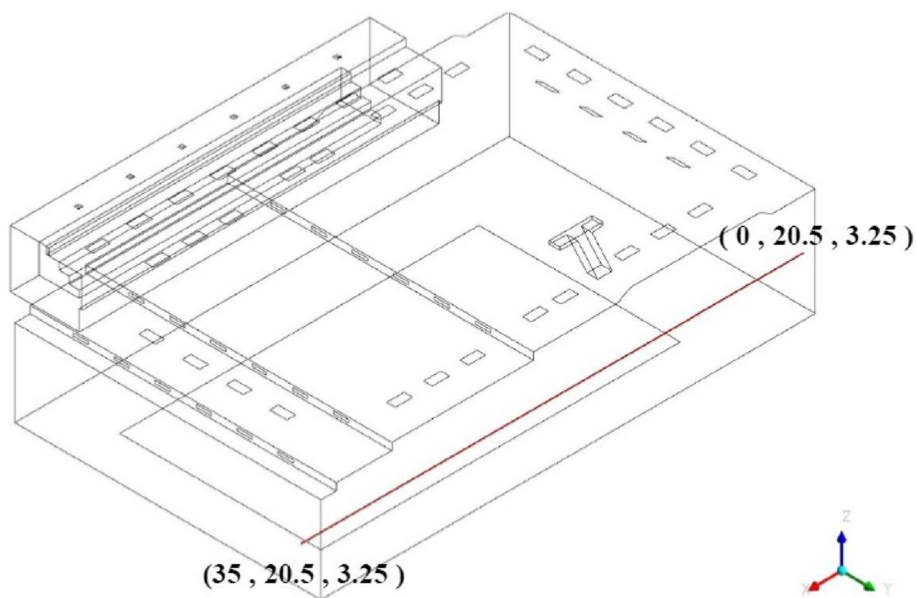


**Fig. 4** Line 1 configuration


presents the spectrum of skewness mesh metrics, ranging from excellent to unacceptable, while Table 2 outlines the spectrum for orthogonal quality metrics, ranging from unacceptable to excellent [23].

**Table 1** Skewness mesh metrics spectrum [23]



| Excellent | Very Good | Good      | Acceptable | Bad       | Unacceptable |
|-----------|-----------|-----------|------------|-----------|--------------|
| 0–0.25    | 0.25–0.50 | 0.50–0.80 | 0.80–0.94  | 0.95–0.97 | 0.98–1.00    |

**Table 2** Orthogonal quality mesh metrics spectrum) [23]



| Unacceptable | Bad        | Acceptable | Good      | Very Good | Excellent |
|--------------|------------|------------|-----------|-----------|-----------|
| 0–0.001      | 0.001–0.14 | 0.15–0.25  | 0.20–0.69 | 0.70–0.95 | 0.95–1    |

**Table 3** Orthogonal quality and skewness values for grid sizes) [23]

| Mesh Quality Metrics | Grid sizes  |             |             |            |
|----------------------|-------------|-------------|-------------|------------|
|                      | 3.5 Million | 5.6 Million | 6.9 Million | 10 Million |
| Orthogonal Quality   | 0.34        | 0.37        | 0.36        | 0.39       |
| Skewness             | 0.65        | 0.62        | 0.63        | 0.60       |

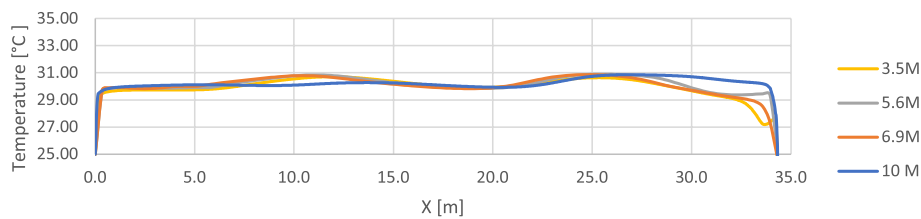


**Fig. 5** Temperature profiles at line 1

To ensure high-quality mesh, the study assessed the orthogonal quality and skewness values for different grid sizes, as shown in Table 3. The evaluated grid sizes were 3.5 million, 5.6 million, 6.9 million, and 10 million. The orthogonal quality values ranged from 0.34 to 0.39, while the skewness values ranged from 0.60 to 0.65 [23].

By carefully assessing mesh quality, this study ensured the reliability and accuracy of the CFD simulations. The chosen mesh size of 5.6 million elements balanced computational efficiency without compromising the quality of the results. The findings of this study contribute to the methodology of meshing in CFD simulations, providing insights into selecting appropriate mesh sizes for similar investigations in the future.

A thorough analysis was carried out to determine the effect of different mesh sizes on simulation outcomes. To understand the distribution of temperature, velocity, and relative humidity along this line, four meshes were used, and the temperature profiles at line 1 as shown in Fig. 5, relative humidity profiles at line 1 as shown in Figs. 6 and 7, and velocity profiles at the line as shown in Figure were analyzed.

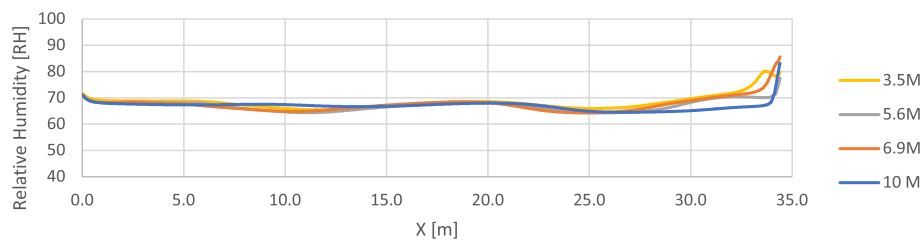


**Fig. 6** Relative humidity profiles at line 1

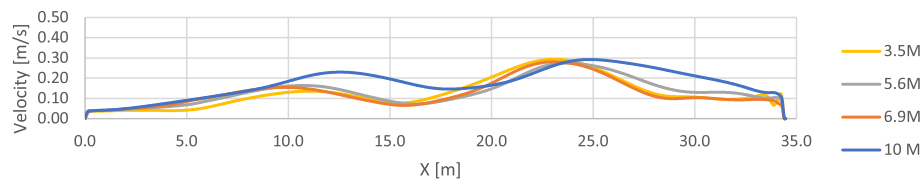


**Fig. 7** Velocity profiles at line 1

The results obtained from the four meshes revealed that there was no significant difference in the profiles. The temperature, velocity, and relative humidity distributions were comparable, indicating that the variations in mesh size did not noticeably affect the overall results.

However, it is important to note that the computing time for the fine mesh was observed to be approximately two times slower compared to the coarser meshes. Considering this trade-off between accuracy and computational efficiency, the 5.6 million mesh size was chosen as the most suitable option for all simulations.

By utilizing the 5.6 million mesh, the study achieved a good balance between accuracy and computational resources. While finer meshes may provide a more detailed resolution of the flow field, the negligible differences observed in the results justified the selection of the 5.6 million mesh size as the preferred choice. This mesh size enabled the study to obtain reliable results within a reasonable computational timeframe.

Overall, the findings demonstrate that the 5.6 million mesh size is a suitable choice for accurately capturing the flow behavior and predicting temperature, velocity, and relative humidity distribution in the indoor swimming pool facility. The optimized mesh size allows for efficient and accurate simulations, thereby enhancing the reliability of the study's conclusions.

### Validation work

A comparison of numerical results generated with ANSYS Fluent software and previously published experimental and numerical results from various researchers in the field who used OpenFOAM software. The goal was to validate the correctness and dependability of the ANSYS Fluent simulations by comparing them to known findings (Real-world data measured and simulated data from OpenFOAM software) [18].

To facilitate the comparison, velocity, and relative humidity profiles were examined at four lines along the X-axis, as depicted in Fig. 8. The specific cartesian coordinates for each line (1, 2, 3, and 4) were determined and are presented in Table 4.

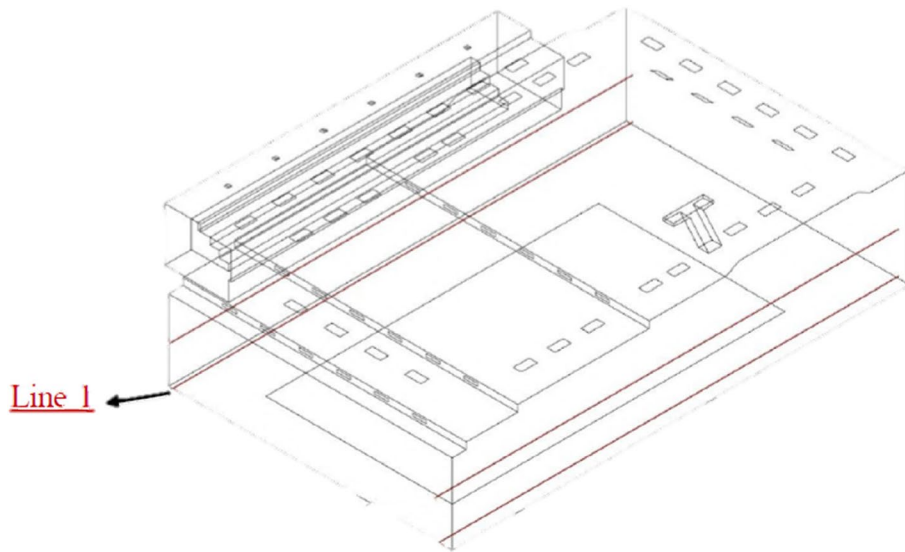


**Fig. 8** Lines 1 location

**Table 4** Cartesian coordinates of lines 1

|        | 1 <sup>st</sup> point |     |     | 2 <sup>nd</sup> point |     |     |
|--------|-----------------------|-----|-----|-----------------------|-----|-----|
|        | X                     | Y   | Z   | X                     | Y   | Z   |
| Line 1 | 0                     | 0.5 | 0.2 | 35                    | 0.5 | 0.2 |

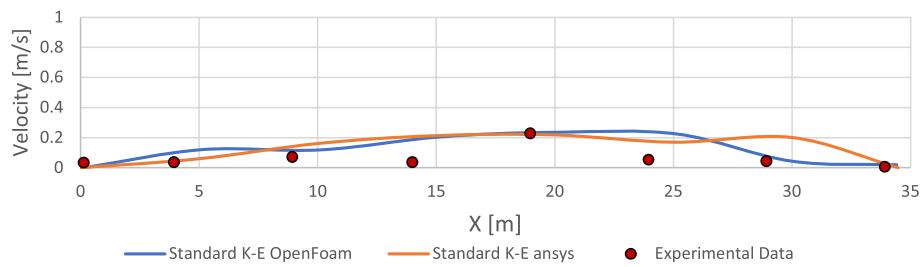


**Fig. 9** Velocity profiles at line 1

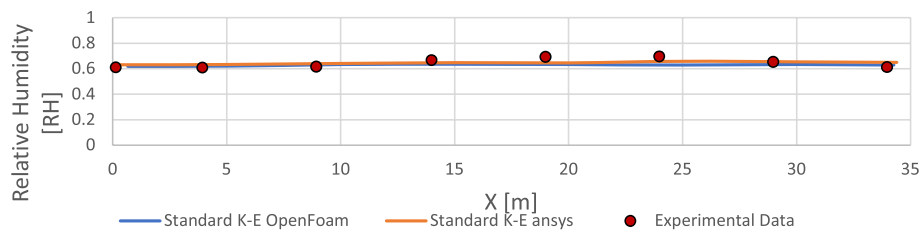


**Fig. 10** Relative humidity profiles at line 1

By analyzing the obtained velocity and relative humidity profiles at these designated lines, a comprehensive evaluation of the simulation results was performed as shown in Figs. 9 and 10. The aim was to determine the level of agreement and consistency between

the ANSYS Fluent simulations and the previously published experimental (Real-world Data) and numerical data. The comparison of the profiles allowed for a thorough assessment of the similarities and differences in the flow behavior and humidity distribution predicted by the two software packages. This analysis contributes to the validation process of the ANSYS Fluent simulations, providing valuable insights into the accuracy of the results concerning the established findings in the field.

Overall, this comparison serves as an important step in verifying the reliability of the numerical simulations conducted in this study. By evaluating the agreement between the ANSYS Fluent results and the previously published experimental and numerical data, the present study ensures the credibility and validity of the obtained findings, thus strengthening the scientific basis of the research. more simulation models implemented in the next section, to improve the ventilation system. All the geometries of the configurations in this next section were created by SpaceClaim software. The 6 configurations compared each other to reach the best design for the location inlet and outlet to achieve thermal comfort for the swimmer and spectator at the lowest ACH recommended by ASHRAE 6 ACH to minimize the energy consumption.

#### **Boundary conditions of the configurations**

The focus of the study improves the thermal comfort in the occupied zone in the hall, located in the area around the swimming pool and spectator stand area, therefore the grilles of the inlet located in this area at different heights and shapes. therefore, to achieve the adequate conditions of thermal and airflow pattern the inlet grilles concentrated in this area with different heights and shapes. The outlet grilles in configuration 1 were in the middle of the ceiling in the swimming pool area and in the side walls of the spectators' stand area.






Also, the inlet grilles were at a height of 3 m from the floor in the side walls of the swimming pool and at the back wall of the spectator area. Configuration 2 outlet grilles located in the ceiling at the spectator stand area to investigate the effect of changing outlet position. Configuration 3 The inlet grilles changed to be 30 cm height from the floor at the swimming pool area. Configuration 4 The inlet grilles in the spectator stand area changed to the fence at 30 cm. To study the effect of shape change configuration 5 used a circular inlet as recommended by ASHRAE at the ceiling, and Configuration 6 was studied the combination of best results from Configuration 1 to Configuration 5 to achieve suitable thermal comfort for the hall, the description of the 6 configuration shown in Table 5.

#### **The inlet air conditions**

##### ***Configurations 1, 2, 3, and 4***

The inlet air conditions for configurations 1, 2, 3, and 4 were consistent in terms of the size, shape, and boundary conditions of the inlet grilles. Table 6 provides the boundary conditions of the inlet, which had dimensions of 1.80 m × 0.20 m. The hydraulic diameter was calculated as 0.36 m. The inlet grilles were associated with 32 inlets. The specified inlet air conditions for the simulations were Temperature: 16 °C and Specific humidity: 0.00563 kg/kg.

**Table 5** The description of the 6 configurations

| Configuration No | Inlet   |                           |             | Outlet   |  |  | Solution  |                           |             |                                       |                                       |   |
|------------------|---|---------------------------|-------------|--|--|--|---|---------------------------|-------------|---------------------------------------|---------------------------------------|---|
|                  | Shape   | Dimension                 | No. of unit | Location   | Water pool area  | Spectator stands                       | Shape   | Dimension                 | No. of unit | Location                              | Water pool area                       | Spectator stands area   |
| 1                |    | 1.80 × 0.20m <sup>2</sup> | 32          | 26 units in the 4 walls of the water pool area at 3 m height   | 26 units in the 4 walls of the water pool area at 3 m height   | 6 unit in the east wall at 3 m heights |  | 1.20 × 0.60m <sup>2</sup> | 12          | 8 in the ceiling above the water pool | 8 in the ceiling above the water pool | 2 on each side of the north wall and south wall<br>4 in the ceiling |
| 2                |   |                           |             |  |  | 6 unit in the ceiling                  |   |                           |             |                                       |                                       |   |
| 3                |   |                           |             | 26 units in the 4 walls of the water pool area at 0.3 m height | 26 units in the 4 walls of the water pool area at 0.3 m height | 6 unit in the ceiling                  |   |                           |             |                                       |                                       |   |
| 4                |   |                           |             | 46 units in the ceiling above the floor area                   | 46 units in the ceiling above the floor area                   | 22 unit in the ceiling                 |   |                           |             |                                       |                                       |   |
| 5                |    | 14"                       | 68          |  |  |  |   |                           |             |                                       |                                       |   |
| 6                |   | 14"                       | 22          | --   | --   | 22 unit in the ceiling                 |   |                           |             |                                       |                                       |   |
|                  |  | 1.80 × 0.20m <sup>2</sup> | 26          | 26 units in the 4 walls of the water pool area at 3 m height   | 26 units in the 4 walls of the water pool area at 3 m height   | --                                     |   |                           |             |                                       |                                       |   |





**Table 6** Boundary conditions of the inlet 1.80 m × 0.20 m

| Type           | Velocity inlet | Hydraulic diameter | 0.36 m        |
|----------------|----------------|--------------------|---------------|
| Length × width | 1.80m × 0.20m  | Temperature        | 16 °C         |
| No. of inlet   | 32             | Specific humidity  | 0.00563 kg/kg |

To determine the velocity of the supply air based on the desired Air Changes per Hour (ACH), calculations were performed. Table 7 presents the calculations for different ACH values, providing the corresponding volume flow rate, inlet area, and velocity.

For example, when considering an ACH of 6, the corresponding volume flow rate was calculated as 20,357 m<sup>3</sup>/h, which is equivalent to 34,586 CFM. The inlet area was determined as 10 m<sup>2</sup>, resulting in a velocity of 0.83 m/s.

**Configuration 5**

Configuration 5 utilized a circular inlet shape, specifically the biggest standard size located at the ceiling as recommended by ASHRAE. the boundary conditions associated with the circular inlet shape, which had a diameter of 14". The inlet was associated with 64 inlets. The specified boundary conditions for the circular inlet shape in Configuration 5 were Temperature: 16 °C and Specific humidity: 0.00563 kg/kg to determine the velocity of the supply air based on the desired Air Changes per Hour (ACH), calculations were performed. Table 8 presents the calculations for different ACH values, providing the corresponding volume flow rate, inlet area, and velocity, when considering an ACH of 6, the corresponding volume flow rate was calculated as 20,357 m<sup>3</sup>/h, which is equivalent to 34,586 CFM. The inlet area was determined as 10 m<sup>2</sup>, resulting in a velocity of 1.42 m/s.

These specified boundary conditions and corresponding calculations were crucial in determining the supply air velocity for Configuration 5, ensuring appropriate air exchange rates and ventilation within the indoor swimming pool facility. The use of a circular inlet shape in this configuration aimed to optimize airflow distribution and achieve the desired thermal comfort and air quality outcomes.

**Table 7** Calculation of velocity of the supply air according to ACH for configuration 1,2,3 and 4

| ACH | Volume m <sup>3</sup> | Volume flow rate |                    |                   | Inlet area m <sup>2</sup> | Velocity m/s |
|-----|-----------------------|------------------|--------------------|-------------------|---------------------------|--------------|
|     |                       | CFM              | m <sup>3</sup> /hr | m <sup>3</sup> /s |                           |              |
| 6   | 5764                  | 20,357           | 34,586             | 10                | 0.36                      | 0.83         |

**Table 8** Calculation of velocity of the supply air according to ACH for Configuration 5

| ACH | Volume m <sup>3</sup> | Volume flow rate |                    |                   | Inlet area m <sup>2</sup> | Velocity m/s |
|-----|-----------------------|------------------|--------------------|-------------------|---------------------------|--------------|
|     |                       | CFM              | m <sup>3</sup> /hr | m <sup>3</sup> /s |                           |              |
| 6   | 5764                  | 20,357           | 34,586             | 10                | 0.099                     | 1.42         |

**Table 9** Boundary conditions of the inlet 1.80 m × 0.20 m for Configuration 6

| Type           | Velocity inlet  | Hydraulic diameter | 0.36 m        |
|----------------|-----------------|--------------------|---------------|
| Length × width | 1.80 m × 0.20 m | Temperature        | 16 °C         |
| No. of inlet   | 26              | Specific humidity  | 0.00563 kg/kg |

**Table 10** Calculation of velocity of the supply air according to ACH for Configuration 6

| ACH | Volume $m^3$ | Volume Flow Rate |          |         | Inlet area<br>$m^2$ | Velocity<br>$m/s$ |
|-----|--------------|------------------|----------|---------|---------------------|-------------------|
|     |              | CFM              | $m^3/hr$ | $m^3/s$ |                     |                   |
| 6   | 5376         | 18,985           | 32,256   | 9       | 0.36                | 0.96              |

**Table 11** Calculation of velocity of the supply air according to ACH

| ACH | Volume $m^3$ | Volume Flow Rate |          |         | Inlet area<br>$m^2$ | Velocity<br>$m/s$ |
|-----|--------------|------------------|----------|---------|---------------------|-------------------|
|     |              | CFM              | $m^3/hr$ | $m^3/s$ |                     |                   |
| 6   | 5376         | 18,985           | 32,256   | 9       | 0.36                | 0.96              |

**Table 12** Boundary conditions of the circular inlet shape 14"

| Type         | Velocity inlet | Hydraulic diameter | 14"           |
|--------------|----------------|--------------------|---------------|
| Diameter     | 14"            | Temperature        | 16 °C         |
| No. of inlet | 22             | Specific humidity  | 0.00563 kg/kg |

### Configuration 6

Configuration 6 was determined based on a comprehensive comparison of the other configurations, taking into consideration the location and shape of the inlet and outlet. The aim was to optimize the ventilation system for enhanced thermal comfort and indoor air quality.

Table 9 presents the boundary conditions for the inlet in Configuration 6. The inlet had dimensions of 1.80 m × 0.20 m, a hydraulic diameter of 0.36 m, and was associated with 26 inlets. The specified boundary conditions included a temperature of 16 °C and a specific humidity of 0.00563 kg/kg.

Velocity calculations for the supply air were performed based on the desired Air Changes per Hour (ACH) values. Table 10 provides the corresponding volume flow rate, inlet area, and velocity for Configuration 6. For instance, when considering an ACH of 6, the volume flow rate was determined as 18,985  $m^3/h$  (equivalent to 32,256 CFM), the inlet area was 9  $m^2$ , and the resulting velocity was 0.96 m/s.

Additionally, Tables 11 and 12 outline the boundary conditions for the circular inlet shape in Configuration 6, which had a diameter of 14". The circular inlet shape consisted of 22 inlets and had the same temperature and specific humidity values as the previous configurations.

The velocity calculations for the circular inlet shape were performed according to the desired ACH values, an ACH of 6, the volume flow rate was 1,371 m<sup>3</sup>/h (equivalent to 2,330 CFM), the inlet area was 0.65 m<sup>2</sup>, and the resulting velocity was 0.30 m/s.

These specified boundary conditions and corresponding calculations played a crucial role in determining the supply air velocity and achieving the desired air exchange rates for Configuration 6. The optimized location and shape of the inlet and outlet in this configuration aimed to enhance thermal comfort and indoor air quality in the indoor swimming pool facility.

The location and the shape of the inlet and the outlet in configuration 6 are taken from comparing the other configurations together.

### The outlet air conditions

The outlet air conditions were consistent across all configurations in terms of the number of outlet units and size, but the position varied. The outlets had the same dimensions with a length of 1.2 m and a width of 0.60 m. The outlet type was specified as a pressure outlet with a hydraulic diameter of 0.8 m. The number of outlets in each configuration was 12. The boundary conditions of the outlets, including their dimensions and hydraulic diameter. The outlets serve as the means for air to exit the indoor swimming pool facility, allowing for proper airflow circulation and ventilation.

By maintaining consistent outlet specifications while altering their positions in each configuration, the study aimed to assess the impact of outlet location on the overall airflow patterns, thermal conditions, and indoor air quality within the indoor swimming pool facility. The variations in outlet positions allowed for the evaluation of different ventilation strategies and their effects on the desired outcomes of thermal comfort and air quality.

### The lighting

The lighting units in the indoor swimming pool facility were treated as hot faces, providing a uniform heat flux to the surrounding atmosphere. Table 13 outlines the boundary conditions of the lighting units, including their dimensions, type, and heat flux. The lighting units had a length of 1.2 m and a width of 0.60 m. They were considered wall-type elements, contributing a heat flux of 2 W/m<sup>2</sup>. The facility consisted of a total of 32 lighting units.

### The walls

The walls in the indoor swimming pool facility were assigned specific boundary conditions to simulate different scenarios. Table 14 provides the boundary conditions for the interior and exterior walls. The facility had two interior walls located on the east and south sides, and two exterior walls situated on the north and west sides. During the summer season, the interior walls were assigned a temperature of 35 °C, while the exterior walls had a higher temperature of 40 °C. These temperature conditions represent the thermal conditions associated with each wall's location and exposure to external heat sources.

**Table 13** Boundary conditions of the lighting unit

| length | Width  | Type | Heat flux          | No. of the lighting unit |
|--------|--------|------|--------------------|--------------------------|
| 1.2 m  | 0.60 m | Wall | 2 W/m <sup>2</sup> | 32                       |

**Table 14** Boundary conditions of the walls

| Type           | No. of wall | Conditions | Temperature | Location             |
|----------------|-------------|------------|-------------|----------------------|
| Interior walls | 2           | Summer     | 35 °C       | East and south sides |
| Exterior walls | 2           | Summer     | 40 °C       | North and west sides |

**Evaporate rate from the pool**

The evaporation rate of the water in the swimming pool is calculated to the lowest air temperature, and the highest water temperature can be, Using the larger of Eqs. (13) and (14) [16].

$$E_0 = C\rho_w(\rho_r - \rho_w)^{\frac{1}{3}}(w_w - w_r) \tag{13}$$

$$E_0 = b(p_w - p_r) \tag{14}$$

where:

$$C = 35$$

$$b = 0.00005$$

$w$  = specific humidity of air, kg of moisture/kg of air

$E_0$  = rate of evaporation from unoccupied pools, kg/m<sup>2</sup>·h

$p$  = partial pressure of water vapor in the air, Pa

$\rho$  = density of air, mass of dry air per unit volume of moist air, kg/m<sup>3</sup>

**Subscripts**

- r = at room temperature and humidity
- w = saturated at water surface temperature

Figure 11 presents valuable insights into the evaporation rate from unoccupied indoor swimming pools. This figure illustrates the evaporation rate, measured in kilograms per square meter per hour (kg/m<sup>2</sup>·h), as it relates to the indoor air temperature and relative humidity levels of 50% and 60%. The data depicted in this figure offers a clear visualization of the impact of air temperature and relative humidity on the rate of water evaporation within indoor pool environments. It is evident that as air temperature decreases or relative humidity decreases, the evaporation rate tends to increase. This relationship is of significant importance for indoor pool management and control of environmental conditions, as it can help inform strategies to mitigate water loss and optimize the indoor swimming experience.

The boundary conditions as shown in Table 15 established at the air–water interface are based on the stability of the saturated vapour layer that forms just above the water surface. The multi-component flow model (species transport, ANSYS Fluent [23] was used to simulate humid air.

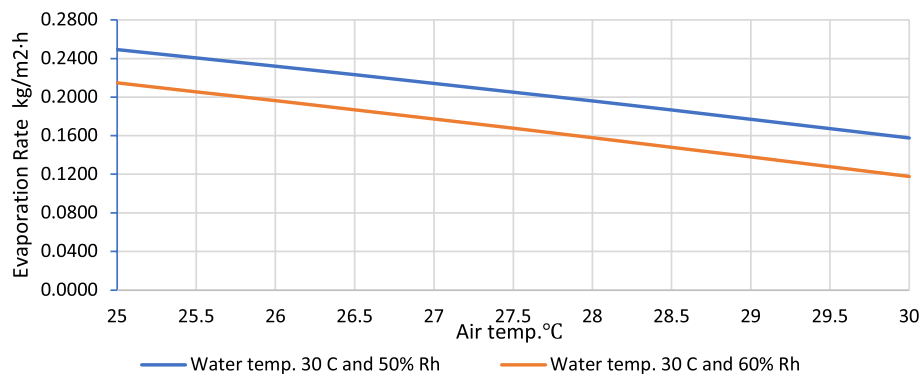


**Fig. 11** Evaporation rate from unoccupied indoor swimming pools

**Table 15** Boundary conditions of the pool

| Type               | Mass flow inlet | Temp. of water | 30 °C            |
|--------------------|-----------------|----------------|------------------|
| Width              | 14 m            | Temp. of air   | 16 °C            |
| Hydraulic diameter | 18 m            | Length scale   | 12.5 m           |
| Length             | 25 m            | Mass flux      | 0.02421Kg/s [16] |

**Results**

The simulated results of the six configurations were evaluated at two planes along the X-axis and four planes along the Y-axis. These planes allowed for a comprehensive analysis of the thermal conditions and predicted comfort parameters within the indoor swimming pool facility.

Figure 12 provides a visual representation of the geometry, indicating the locations of the planes along the X-axis. The "Plane X" is positioned at X = 18 m, which corresponds to the middle of the hall along the YZ planes. This location enables the assessment of temperature, velocity, and other parameters in the central area of the facility. And Fig. 13 illustrates the geometry with the plane Y, representing the locations along the Y-axis. The "Plane Y" is located at Y = 11 m, positioned at the middle of the hall and the diving stand along the XZ planes. This plane facilitates the evaluation of thermal conditions and airflow patterns in the middle section of the facility, including the diving area.

The simulation results of velocity compared at seven planes for all configurations within minimum velocity (0 m/s) and maximum velocity (1.49 m/s) as shown in Figs. 14 and 15.

The simulation results of temperature compared at seven planes for all configurations within a minimum temperature (16 °C) and maximum temperature (40 °C) as shown in Figs. 16 and 17.

The simulation results of relative humidity compared at seven planes for all configurations within minimum relative humidity (17 RH%) and maximum relative humidity (50 RH%) as shown in Figs. 18 and 19.

Indoor air quality and thermal comfort are closely related. Studies have shown that factors such as temperature, humidity, air movement, and pollutants can affect

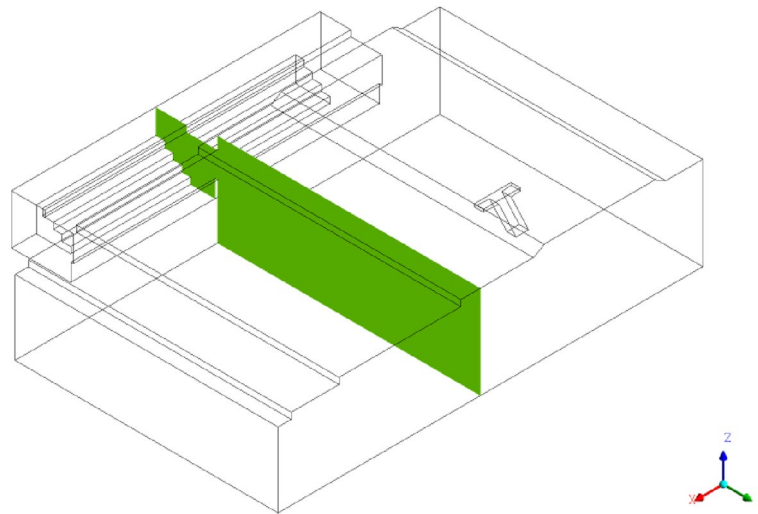


**Fig. 12** View of the geometry shown the plane X locations on the X-axis(18 m)

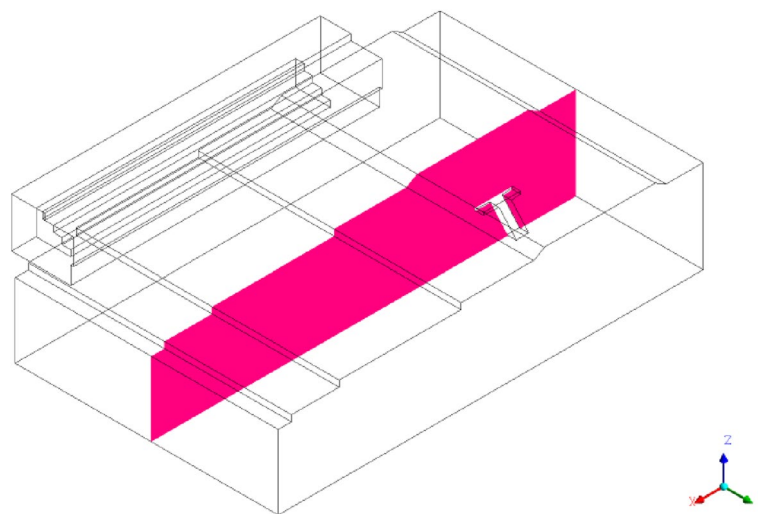


**Fig. 13** View of the geometry shown the plane Y- locations on the Y-axis(11 m)

occupants' perception of comfort. Higher relative and absolute air humidity, as well as moisture load, have been associated with perceptions of unstable room temperature, too low room temperature, stuffy air, and unpleasant odor [24]. Additionally, Air quality perception, including factors such as CO<sub>2</sub> levels, is influenced by thermal, air movement, and humidity sensation, rather than just CO<sub>2</sub> alone [25]. Overall, maintaining good indoor air quality is crucial for ensuring occupants' thermal comfort and satisfaction [26]. To assess the thermal comfort levels within the indoor swimming pool facility, Fanger [27] proposed the Predicted Mean Vote (PMV), and it is defined as an index that anticipates the mean reaction of a large group of people based on the ASHRAE thermal sensation scale. PMV can be estimated using the six essential thermal environment factors, which represent combinations of environmental and

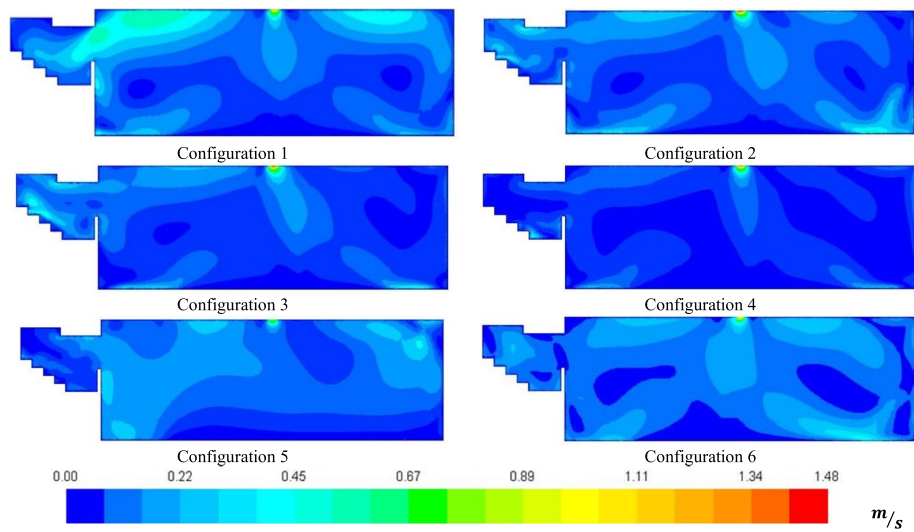


**Fig. 14** Simulation result of velocity at plane X-2

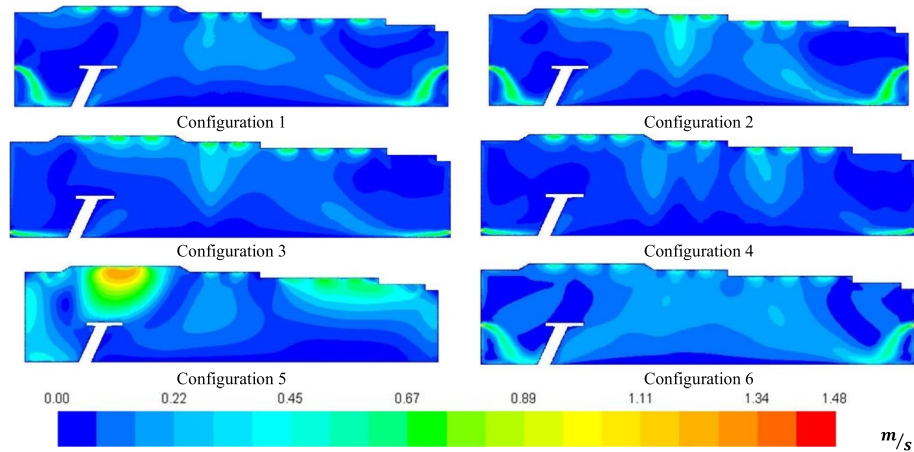


**Fig. 15** Simulation result of velocity at plane Y

personal data, as specified in ASHRAE Standard 55 [28]. the Predicted Mean Vote (PMV) and Predicted Percentage of Dissatisfied (PPD) parameters were calculated. The PMV is determined using the Eq. (15):

$$\begin{aligned}
 PMV = & \left[ 0.352e^{-0.042M} + 0.032 \right] (M - 0.35(43 - 0.061M - Pa) \\
 & - 0.42(M - 50) - 0.0023M(44 - Pa) - 0.0014M(34 - T_a) \\
 & - 3.4 \times 10^8 f_{cl} \left( (T_b + 273)^4 - (T_a + 273)^4 \right) - f_{cl} h (T_b - T_a) \quad (15)
 \end{aligned}$$

$$PPD = 100 - 95e^{-[0.03353PMV^4 + 0.2179PMV^2]} \quad (16)$$



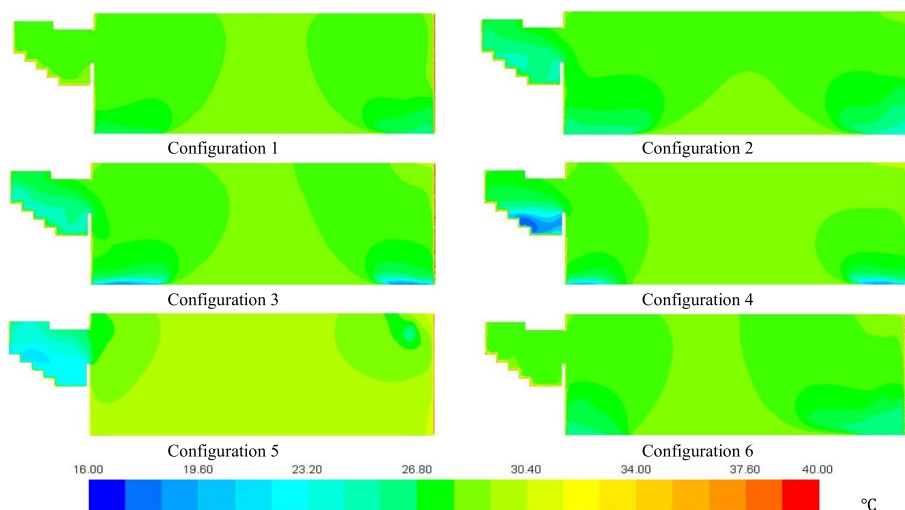


Fig. 16 Simulation result of temperature at plane X

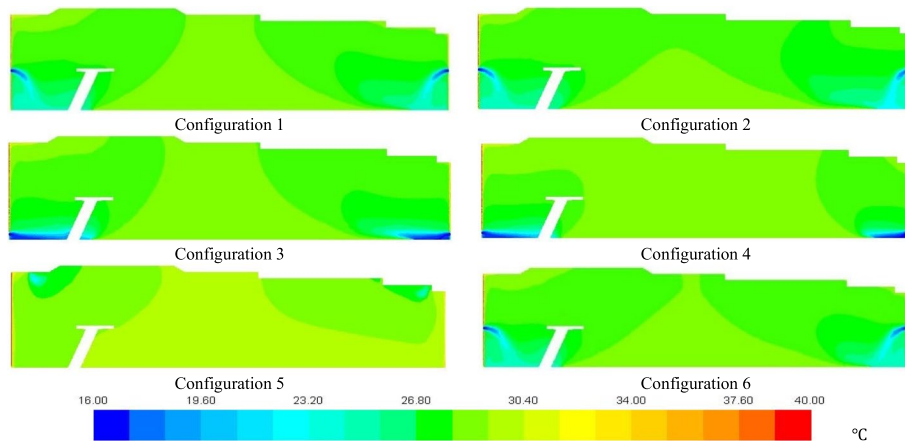


Fig. 17 Simulation result of temperature at plane Y

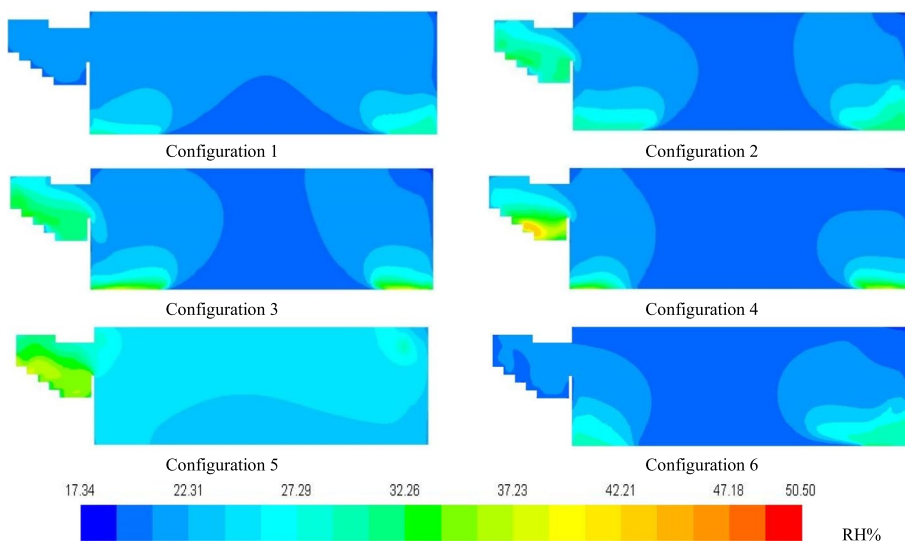
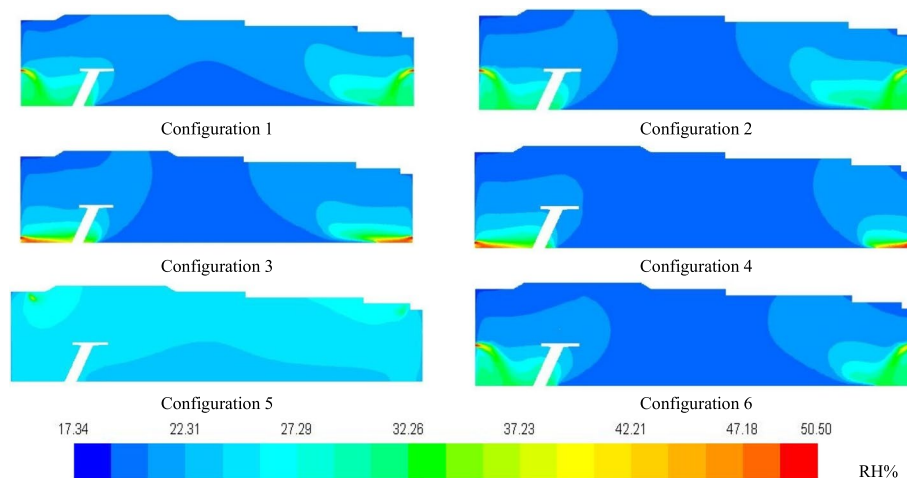


Fig. 18 Simulation result of relative humidity at plane X



**Fig. 19** Simulation result of relative humidity at plane Y

where:

PMV = Predicted mean vote; PPD = Predicted percentage of dissatisfied,  $M = \text{Metabolic rate} = 43.741 \frac{\text{Kcal}}{\text{m}^2 \cdot \text{hr}}$ ;  $P_a = \text{vapor pressure, mmHg}$ ;  $T_a = \text{air temperature near surface, } ^\circ\text{C}$ ;  
 $T_b = \text{Body surface Temperature } ^\circ\text{C}$  ;  $F_{cl} = \text{clothing area factor } 1.15$  ;  $H = 8.95 V^{.5} = \text{Heat transfer coefficient, } \frac{\text{Kcal}}{\text{hr} \cdot \text{m}^2 \cdot ^\circ\text{C}}$  and  $V = \text{Local air velocity, m/s}$ .

These equations allow for the evaluation of thermal comfort levels based on various parameters, providing insights into the occupants’ likely perception of the thermal conditions within the indoor swimming pool facility. Figure 20 shows the simulation results of PMV compared at seven planes for all configurations within the minimum PMV (-0.87) and highest PMV (4.37).

And Fig. 21 depicts the simulation results of PPD compared at seven planes for all configurations within the minimum PPD (5) and maximum PPD (100).

### Discussion

The comparison between the Standard K-ε Ansys simulation and the experimental data revealed an acceptable level of agreement, indicating the reliability of the simulation results. Furthermore, the simulation using Ansys demonstrated better performance in several comparisons when compared to the simulation using OpenFOAM. One notable difference was in the treatment of the boundary condition for water vapor evaporating from the pool surface. The Ansys simulation employed a mass flow rate from the pool surface, as suggested by M. M. Shah, which resulted in a more accurate representation of the evaporative rate compared to the assumption of an air layer with 100% relative humidity at 29 °C used in the OpenFOAM simulation.

The hottest temperature zone was found to be centered around both the spectators’ area and the pool basin, which had a lower temperature. The presence of extra light sources near the spectator area may be contributing to this high temperature. Due to the evaporate rate of the water in the pool, the air temperature in the pool is higher than any other temperatures within and outside its boundaries. The presence of supply air jets close to the ceiling caused the temperature to drop further away from the pool.

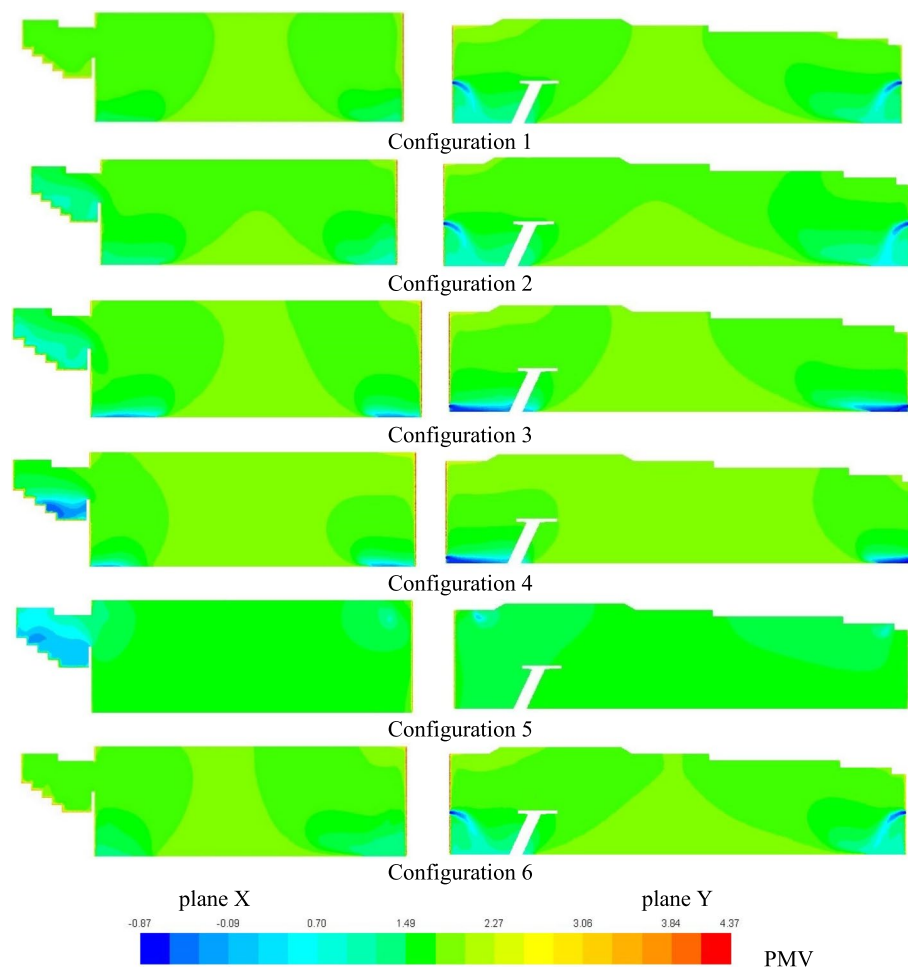


**Fig. 20** Simulation result of PMV

The results show how relative humidity changed as the number of spectators increased. For the same water vapor concentration, relative humidity decreases as temperature rises. This is because colder air requires less moisture to get saturated than warmer air.

the comprehensive examination of diverse configuration scenarios has yielded profound insights into the thermal comfort and indoor air quality dynamics within the context of the swimming pool facility. Configuration 1's discernible reduction in PMV and PPD levels at the periphery of the spectator stand area, attributed to strategic outlet grille placements, is noteworthy. Furthermore, the superior PMV and PPD outcomes in the swimming pool area compared to the spectator stand area underscore the impact of layout variations.

Transitioning to Configuration 2, the relocation of outlet grilles to the ceiling engendered consistent PMV results in the swimming pool area and exhibited enhancements in the spectator stand area. Configuration 3 sustained uniformity in the spectator stand area due to unchanged inlet and outlet grille positions, albeit at the cost of escalated PMV and PPD values relative to Configurations 1 and 2, due to the lower positioning of the inlet grille at 30 cm.

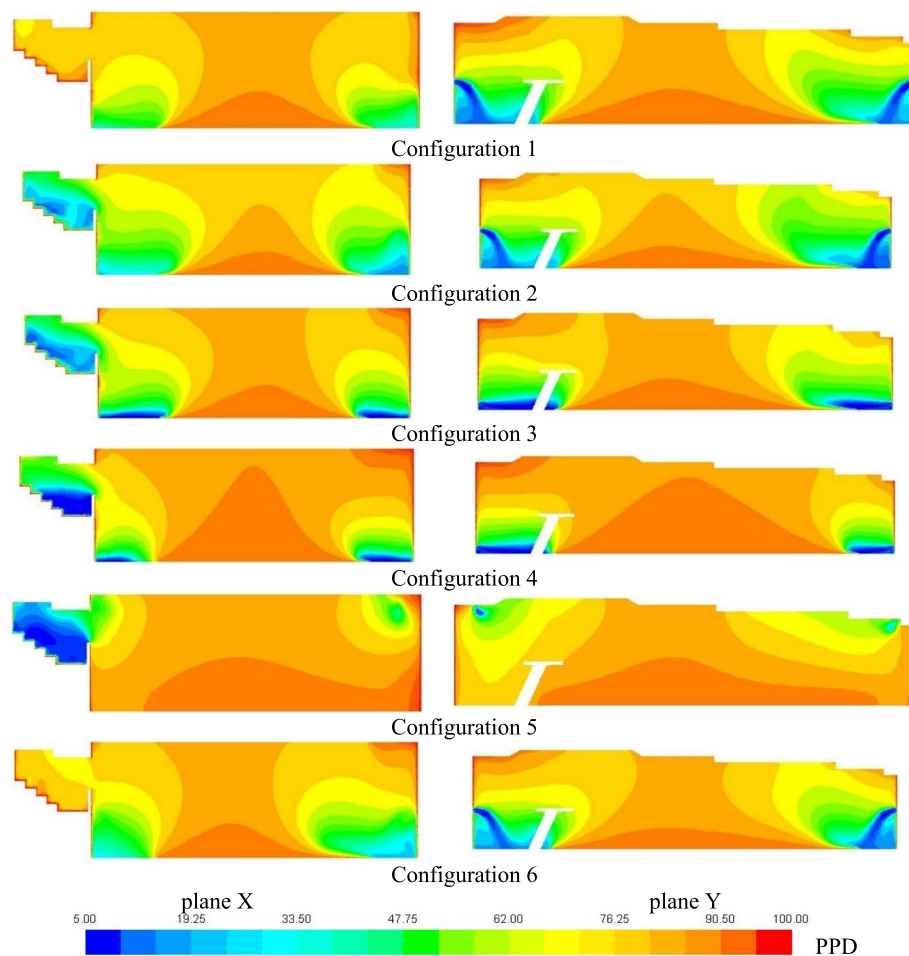


**Fig. 21** Simulation result of PPD

Configuration 4's emulation of Configuration 3's swimming pool area PMV values was counterbalanced by elevated PMV and PPD readings in the spectator stand area, arising from the lower positioning of inlet grilles near the fencing. Configuration 5's distinctiveness lay in reduced PPD levels in the spectator stand area and elevated PPD in the hall, a manifestation of the interplay between low-speed inlet air and the hall's vertical dimensions, leading to non-uniform air distribution.

In stark contrast, Configuration 6 exemplified optimal PMV and PPD outcomes, exemplifying thermal comfort conditions across the entire hall. This configuration's triumph underscores the pivotal role of meticulous outlet and inlet grille placement, coupled with considerations of inlet air velocity and holistic hall design, in achieving the pinnacle of indoor thermal comfort and air quality.

## Conclusions

This study utilized CFD simulations with ANSYS Fluent 17.2 to investigate the flow regimes, temperature distributions, and relative humidity profiles inside an indoor swimming pool. The simulation approach successfully solved the continuity,

momentum, energy, and species transport equations, as well as the k-epsilon turbulence closure model. A mesh size exceeding 5.6 million elements was employed, enabling accurate predictions of the flow regimes and contributing to meaningful results.

The major conclusions drawn from this study are as follows:

- The validation results demonstrated a satisfactory agreement between the results obtained using ANSYS Fluent 17.2 and those obtained using OpenFOAM software, further confirming the reliability of the ANSYS simulation approach.
- In the comparison between configurations 5 and 2, it was observed that the circular inlet in the ceiling, coupled with a low-speed air supply, exhibited superior performance in the spectator stand area compared to the rectangular inlet.
- The comparison between configurations 5 and 2 also revealed that the rectangular inlet in the side walls of the swimming pool area displayed better performance than the circular inlet when considering a low-speed air supply. This can be attributed to the height of the hall and its influence on the airflow patterns.
- The thermal comfort results indicated that lower inlet grille heights, as seen in configurations 1 and 2 compared to configurations 3 and 4, resulted in lower thermal comfort levels. This highlights the importance of considering the positioning and height of the inlet grilles for optimal thermal comfort.
- Configuration 6 emerged as the best design for the swimming pool hall, based on the acceptable range of Predicted Mean Vote (PMV) and Predicted Percentage of Dissatisfied (PPD), indicating favorable thermal comfort conditions.
- A design solution involving a glass partition is proposed to address challenges like water evaporation rate and high relative humidity for spectators. This separation creates a physical boundary, allowing spectators to enjoy unobstructed views of the swimming pool while shielding them from discomfort. The transparent glass wall provides better indoor air quality and thermal conditions, enhancing spectator comfort and overall experience. The viability of this design concept can be assessed through detailed simulations, ensuring its effectiveness in improving indoor air quality and thermal comfort.

Future research could focus on incorporating transient simulations and dynamic conditions into the analysis of indoor swimming pool environments. Exploring the effects of varying occupancy patterns, changing weather conditions, and fluctuating evaporate rates within a time-dependent framework could provide a more accurate representation of real-world scenarios. By considering these dynamic factors, the study could offer a deeper understanding of how indoor air quality and thermal comfort interact with evolving conditions, ultimately leading to more precise predictions and actionable insights for optimal pool facility design and operation.

### **Nomenclature**

$A$  = surfaces of the control volume

$b = 0.00005 = \text{Constant}$

$C = 35 = \text{Constant}$

$E_0$  = rate of evaporation from unoccupied pools,  $\text{kg/m}^2 \cdot \text{h}$

$E_o$  = rate of evaporation from an occupied swimming pool,  $\frac{\text{kg}}{\text{m}^2 \cdot \text{h}}$   
 $E_{occ}$  = rate of evaporation from an occupied swimming pool  $\frac{\text{kg}}{\text{m}^2 \cdot \text{h}}$   
 $F_{cl}$  = clothing area factor 1.15  
 $g$  = Gravitational acceleration,  $\text{m/s}^2$   
 $H = 8.95 V^{.5}$  = Heat transfer coefficient,  $\frac{\text{Kcal}}{\text{hr} \cdot \text{m}^2 \cdot ^\circ\text{C}}$   
 $h$  = Enthalpy,  $\text{kJ/kg}$   
 $k$  = Thermal conductivity coefficient,  $\text{W/m}^\circ\text{C}$   
 $M$  = Metabolic rate =  $43.741, \frac{\text{Kcal}}{\text{m}^2 \cdot \text{hr}}$   
 $N$  = the number of occupants per unit pool area  
 $\hat{n}$  = the unit normal vector  
 $p$  = partial pressure of water vapor in the air, Pa  
 $P_a$  = vapor pressure, mmHg  
 $T$  = Drybulb Temperature of gas mixture, K  
 $T_a$  = air temperature near surface,  $^\circ\text{C}$   
 $T_b$  = Body surface Temperature  $^\circ\text{C}$   
 $t$  = Time, s  
 $\tau_{ij}$  = Subgrid – scale stress  
 $u$  = Instantaneous velocity component in x direction,  $\text{m/s}$   
 $v$  = the fluid velocity,  $\text{m/s}$   
 $V$  = Local air velocity,  $\text{m/s}$   
 $v$  = Instantaneous velocity component in y direction,  $\text{m/s}$   
 $w$  = Instantaneous velocity component in z direction,  $\frac{\text{m}}{\text{s}}$   
 = specific humidity of air, kg of moisture/kg of air  
 $x, y, z$  = Cardinal coordinate components  
 $Y$  = the water vapor mass fraction (kg of water vapor/kg of humid air)  
 $\rho$  = Density,  $\text{kg/m}^3$

#### Abbreviations

|        |   |
|--------|---|
| ACH    | Air Changes per Hour  |
| ASHRAE | American Society of Heating, Refrigerating and Air-Conditioning Engineers |
| CFD    | Computational Fluid Dynamics  |
| IAQ    | Indoor air quality  |
| PMV    | Predicted Mean Vote   |
| PPD    | Predicted Percentage of Dissatisfied                                      |

#### Acknowledgements

Not applicable.

#### Authors' contributions

AH, MI, TA and SM contributed to the design and implementation of the research, to the analysis of the results and to the writing of the manuscript.

#### Funding

This research received no specific grant from any funding agency in the public, commercial, or not-for-profit sectors.

#### Availability of data and materials

The datasets used and/or analyzed during the current study are available from the corresponding author on reasonable request.

#### Declarations

##### Competing interests

The authors declare that they have no competing interests.

Received: 11 July 2023 Accepted: 25 August 2023

Published online: 30 September 2023

**References**

1. Carlos S, Joana F, Ana I, Miranda. (2019) The challenges of air quality modelling when crossing multiple spatial scales. *Air Qual Atmos Health* 12(9):1003–1017. <https://doi.org/10.1007/S11869-019-00733-5>
2. Belis C, Blond N, Bouland C, Carnevale C, Clappier A, Douros J, & Volta M (2017) Strengths and weaknesses of the current EU situation. air quality integrated assessment: a European perspective, 69–83.
3. Rubio-Herrero J, Marrero CO, Fan WTL (2020) Modeling atmospheric data and identifying dynamics: temporal data-driven modeling of air pollutants. arXiv: Applications,
4. Indranil B (2014) Advantages and applications of transforming empirical model input space with dimensional models. *Int J Engine Res*. <https://doi.org/10.1177/1468087414523420>
5. Rasha, Shakir, AbdulWahhab., Karan, Jetly, Shqran, Shakir. (2021). Indoor air quality monitoring systems: a comprehensive review of different IAQM Systems. doi: <https://doi.org/10.4018/IJKBO.2021070101>
6. Ahmet Ç (2020) Determination of indoor air quality in collective living spaces utilizing Fuzzy logic analysis. *Revista De La Construcción*. <https://doi.org/10.7764/RDLC.19.3.288-300>
7. Blázquez JLF, Maestre IR, Gallero FJG, Pérez-Lombard L, Bottarelli M (2023) Experimental adjustment of the turbulent Schmidt number to model the evaporation rate of swimming pools in CFD programmes. *Case Stud Therm Eng* 41:102665
8. Hanafi AM, Ibrahim MA, Abou-deif TM, Morcos SM (2023) CFD validation and verification of airflow characteristics in indoor swimming pool. *World Sci J Mod Res Meth* 2(3):89–104
9. Rojas G, Grove-Smith J (2018) Improving ventilation efficiency for a highly energy efficient indoor swimming pool using CFD simulations. *Fluids* 3(4):92
10. Ciuman P, Lipska B (2018) Experimental validation of the numerical model of air, heat and moisture flow in an indoor swimming pool. *Build Environ* 145:1–13
11. Koper P, Lipska B, Michnol W (2010) Assessment of thermal comfort in an indoor swimming-pool making use of the numerical prediction CFD. *ArchCivil Eng Environ* 3(3):95–103
12. Blázquez JLF, Maestre I (2017) A new practical CFD-based methodology to calculate the evaporation rate in indoor swimming pools. *Energy Build* 149(133):141
13. Incropera F.P, D. D (2011) *Fundamentals of Heat and Mass Transfer* 7th Edition . John Wiley and Sons .
14. Yunus Cengel. (2014). *Heat and mass transfer: fundamentals and applications*. McGraw-Hill Higher Education.
15. Boukadida N, Nasrallah SB (2001) Mass and heat transfer during water evaporation in laminar flow inside a rectangular channel - validity of heat and mass transfer analogy. *Int J Therm Sci* 40(1):67–81
16. Shah MM (2014) Methods for calculation of evaporation from swimming pools and other water surfaces. *ASHRAE*.
17. Abo Elazm M, Shahata AI (2015) Numerical and field study of the effect of air velocity and evaporation rate on indoor air quality in enclosed swimming pools. *Int Rev Mech Eng* 9(1):97
18. Limane A, Fellouah H, Gal N (2017) Simulation of airflow with heat and mass transfer in an indoor swimming pool by OpenFOAM. *Int J Heat Mass Transf* 109:862–878
19. Lebon M, Fellouah H, Galanis N (2016) Numerical analysis and field measurements of the airflow patterns and thermal comfort in an indoor swimming pool: a case study. *Energ Effi* 10(3):527–548
20. Chorin AJ (1990) *A Mathematical Introduction To Fluid Mechanics*. Springer-Verlag, New York
21. White FM, Corfield I (2006) *Viscous fluid flow*. McGraw-Hill, New York
22. Hajdukiewicz M, Geron M (2013) Formal calibration methodology for CFD models of naturally ventilated indoor environments. *Build Environ* 59(290):302
23. ANSYS (2011) *ANSYS Fluent Theory Guide*.
24. Juan W, Dan N (2022) Subjective indoor air quality and thermal comfort among adults in relation to inspected and measured indoor environment factors in single-family houses in Sweden-the BETSI study. *Sci Total Environ*. <https://doi.org/10.1016/J.SCITOTENV.2021.149804>
25. de Oliveira CC, Rupp RF, Ghisi E. (2021). Assessment of air quality perception and its effects on users' thermal comfort in office buildings. <https://doi.org/10.20944/PREPRINTS202106.0324.V>
26. Liming Wu, Haishan X, Xianfeng W, Qingfeng D, Chunxiang L, Xiaotong L, Rui L (2020) Indoor air quality and passenger thermal comfort in Beijing metro transfer stations. *Transp Res D: Transp Environ*. <https://doi.org/10.1016/J.TRD.2019.102217>
27. Fanger PO (1970) *Thermal comfort. Analysis and applications in environmental engineering*. Thermal comfort. Analysis and applications in environmental engineering.
28. ASHRAE A. (2010) *ASHRAE standard 55–2010; Thermal Environmental Conditions for Human Occupancy*. American Society of Heating, Refrigerating, and Airconditioning Engineers, Inc.: Atlanta, GA, USA.

**Publisher's Note**

Springer Nature remains neutral with regard to jurisdictional claims in published maps and institutional affiliations.